

Geometric Impedance Control on $SE(3)$ for Robotic Manipulators

Joohwan Seo* Nikhil Potu Surya Prakash* Alexander Rose**
Jongun Choi*** Roberto Horowitz*

* University of California, Berkeley, CA, 94720 USA

** Leibniz University Hannover, Germany

*** Yonsei University, Seoul, Republic of Korea

e-mail: {joohwan_seo, nikhilps, rose1993, horowitz}@berkeley.edu,
jongunchoi@yonsei.ac.kr

Abstract: After its introduction, impedance control has been utilized as a primary control scheme for robotic manipulation tasks that involve interaction with unknown environments. While impedance control has been extensively studied, the geometric structure of $SE(3)$ for the robotic manipulator itself and its use in formulating a robotic task has not been adequately addressed. In this paper, we propose a differential geometric approach to impedance control. Given a left-invariant error metric in $SE(3)$, the corresponding error vectors in position and velocity are first derived. We then propose the impedance control schemes that adequately account for the geometric structure of the manipulator in $SE(3)$ based on a left-invariant potential function. The closed-loop stabilities for the proposed control schemes are verified using Lyapunov function-based analysis. The proposed control design clearly outperformed a conventional impedance control approach when tracking challenging trajectory profiles.

Keywords: Robotic Manipulators, Autonomous Robotic Systems, Intelligent Robotics, Asymptotic Stabilization, Tracking, Geometric Control, Impedance Control

1. INTRODUCTION

Impedance control was first proposed to solve the manipulator's end-effector positioning problem Hogan (1985). Since then, often combined with an operational space frame formulation Khatib (1987), it has been the main framework for controlling the end-effector position in the Cartesian space, particularly on tasks that involve interaction with the environment, and is thereby widely utilized in robotic manipulation Abu-Dakka and Saveriano (2020).

The end-effector impedance can be configured to ensure safety in interaction-rich tasks. Particularly, impedance control enables an engineering trade-off between positioning accuracy requirements and robustness against unmodeled interactions Chen and Liu (2013); Khan et al. (2010); Ott et al. (2008). To better deal with the unknown environment, impedance control is often combined with learning algorithms; adaptive control approaches such as Li et al. (2010); Duan et al. (2018), behavior cloning approaches including Rozo et al. (2016); Abu-Dakka et al. (2018) and reinforcement learning approaches Zhang et al. (2021); Martín-Martín et al. (2019); Luo et al. (2019).

Tracking errors in the Cartesian space impedance control are often calculated separately as translation and orientation errors in the spatial frame. In Caccavale et al. (1999), representations for the orientation error utilizing rotation matrices are proposed. The concept of using the geometry of $SO(3)$ to define orientation errors is widely employed, e.g., Zhu et al. (2020); Ochoa and Cortesão (2021). However, to date, most schemes utilized for separating translation and orientation errors do not adequately

consider the geometry of $SE(3)$, even though the end-effector lies in $SE(3)$.

In impedance control, three major components address the dynamic behavior between the manipulator and the environment: mass, spring, and damper. Among these components, a spatial spring defined in $SE(3)$ was utilized in robotic applications by Stramigioli and Duindam (2001) and also in the control of Unmanned Aerial Vehicles (UAV) by Rashad et al. (2019). The wrenches from the spatial springs and linear dampers are utilized as the control inputs. Based on a defined spatial spring, the impedance control was derived in Fasse and Broenink (1997) in the spatial frame. Although the manifold structure of $SE(3)$ is considered in these works, results involving time-varying trajectories and a stability analysis were not provided.

Thus, to the best of our knowledge, the intrinsic manifold and geometrical structure of impedance control from the control perspective has not yet been rigorously examined. For example, in general, desired and current Cartesian velocities are directly compared even though they are not in the same tangent spaces of the $SE(3)$ manifold Li et al. (2010); Khan et al. (2010). Additionally, since there is no bi-invariant error metric in $SE(3)$ Park (1995), Bullo and Murray (1995), the position error vectors need to be defined so that they are consistent with the error metric that has been selected. For example, utilizing spatial frame-based error vectors for left-invariant metrics is inconsistent with its geometry, and the performance of the control system can be increased when error vectors are properly defined.

In this paper, we revisit impedance control for robotic manipulators in the context of differential geometry. We first define position and velocity errors in the end-effector body frame lying on its tangent space, followed by two versions of a geometric impedance control law, built upon results from Bullo and Murray (1999). It is shown with a numerical simulation example that our proposed control scheme outperforms conventional non-geometric impedance control approaches in trajectory tracking.

This paper can be considered as an extension of Lee et al. (2010) from $SO(3)$ to $SE(3)$ and from UAVs to robotic manipulators, and is closely related to the geometric control proposed by Bullo and Murray (1999) in the context of Cartesian operation space impedance control. Compared to Lee et al. (2010), which utilizes a scalar gain, we define the rotational potential function utilizing a matrix impedance gain, which is important in the framework of variable impedance control. We provide a justification for formalizing a left-invariant potential function, which is one of the several such functions suggested by Bullo and Murray (1999). In addition, we present complete stability analyses for both controllers, which have been previously omitted for $SE(3)$, while minimizing the use of advanced differential geometric mathematical constructs and notations. We emphasize that using correct error vectors consistent with the task defined in $SE(3)$ will be critical to learning the required variable impedance control gains in many learning assembly operations since this will minimize the detrimental effects during learning caused by erroneous manipulator behavior due to inconsistent error tracking. Furthermore, the left-invariant error vector can be useful in encoding manipulation tasks lying in $SE(3)$.

The paper is organized as follows: Section. 2, presents a brief review of Lie groups in $SO(3)$ and $SE(3)$ and their respective $\mathfrak{so}(3)$ and $\mathfrak{se}(3)$ algebras, as well a brief review of its use in forward kinematics and manipulator dynamics. In Section 3, the error function in $SE(3)$ proposed in this paper and its corresponding error vectors are derived, as well as geometrically consistent impedance control laws. Stability analyses of the corresponding closed-loop systems are provided as well. Section 4 shows the simulation results of the proposed approach. Benchmark results are also presented in comparison to the conventional impedance controller. Finally, concluding remarks and future work are discussed in Section 5.

2. MANIPULATOR DYNAMIC MODEL

2.1 Lie group and Lie algebra of $SO(3)$ and $SE(3)$

In this subsection, we briefly review the contents of group structure and its geometry. For the detailed description regarding Lie group & Lie algebra and their applications to robotics, the reader is referred to Murray et al. (1994) and Lynch and Park (2017). The configuration of a robotic manipulator's end-effector is defined by its position and orientation; the configuration manifold lies in the special Euclidean group $SE(3)$. The homogeneous representation of the $SE(3)$ configuration manifold is given by

$$g = \begin{bmatrix} R & p \\ 0 & 1 \end{bmatrix} \in SE(3). \quad (1)$$

where $R \in SO(3)$, $p \in \mathbb{R}^3$, and $SO(3) = \{R \in \mathbb{R}^{3 \times 3} | R^T R = RR^T = I, \det(R) = 1\}$.

The Lie algebra of $SO(3)$, denoted by $\mathfrak{so}(3)$, defines skew-symmetric matrices. The hat map for $\mathfrak{so}(3)$ is defined by $\widehat{(\cdot)} : \mathbb{R}^3 \rightarrow \mathfrak{so}(3)$, which maps an angular velocity vector $\omega \in \mathbb{R}^3$ to its skew-symmetric cross product matrix i.e., $\widehat{\omega} = -\widehat{\omega}^T$ for $\omega \in \mathbb{R}^3$. Thus, for any vector $v \in \mathbb{R}^3$, $\widehat{\omega}v = \omega \times v$. Whereby an element in $\mathfrak{so}(3)$ can be mapped form a vector in \mathbb{R}^3 using the *hat-map* $\widehat{(\cdot)} : \mathfrak{so}(3) \rightarrow \mathbb{R}^3$. The inverse of the hat map, $\widehat{(\cdot)}$, is the *vee-map* $\widehat{(\cdot)}^\vee : \mathfrak{so}(3) \rightarrow \mathbb{R}^3$. Similarly to $SO(3)$, the Lie algebra of $SE(3)$ is denoted by $\mathfrak{se}(3)$. The *hat-map* for $\mathfrak{se}(3)$ is defined as $\widehat{(\cdot)} : \mathbb{R}^6 \rightarrow \mathfrak{se}(3)$. The inverse map of hat map is defined by *vee-map* $\widehat{(\cdot)}^\vee : \mathfrak{se}(3) \rightarrow \mathbb{R}^6$. Thus,

$$\widehat{\xi} = \begin{bmatrix} \widehat{\omega} & v \\ 0 & 0 \end{bmatrix} \in \mathfrak{se}(3), \quad \forall \xi = \begin{bmatrix} v \\ \omega \end{bmatrix} \in \mathbb{R}^6, \quad v, \omega \in \mathbb{R}^3, \quad \widehat{\omega} \in \mathfrak{so}(3). \quad (2)$$

2.2 Forward Kinematics

We begin this subsection by noting that our interest is in robotic manipulators with revolute joints. We also use the matrix exponential given as

$$e^A = \sum_{k=0}^{\infty} \frac{1}{k!} A^k, \quad A \in \mathbb{R}^{n \times n} \quad (3)$$

to describe the kinematics of the manipulator as in Murray et al. (1994):

$$g(q) = e^{\widehat{\xi}_1 q_1} e^{\widehat{\xi}_2 q_2} \dots e^{\widehat{\xi}_n q_n} g(0) = \begin{bmatrix} R(q) & p(q) \\ 0 & 1 \end{bmatrix} \in SE(3) \quad (4)$$

where $g(q)$ is the homogeneous representation (1) of the end-effector in the spatial frame, $\xi_i \in \mathbb{R}^6$ and $q_i \in \mathbb{R}$ are a twist represented in the spatial frame and a joint angle of the i^{th} joint, respectively, for $i = 1, 2, \dots, n$, and n is the number of joints. In addition, $g(0)$ is an initial configuration. Since we are dealing with revolute joints, the joint generalized coordinate vector is $q = [q_1, \dots, q_n]^T \in \mathbb{S}^n$.

The velocity of the end-effector in the body frame, $V^b \in \mathbb{R}^6$, can be calculated using following formula:

$$\widehat{V}^b = \begin{bmatrix} v^b \\ \omega^b \end{bmatrix} = g^{-1} \dot{g} \quad (5)$$

i.e., $\dot{g} = g \widehat{V}^b$. The velocity V^b can also be computed using the body Jacobian matrix $J_b(q)$ as follows:

$$V^b = J_b(q) \dot{q}. \quad (6)$$

For the details about $J_b(q)$, we refer to Chap 5.1 of Lynch and Park (2017).

2.3 Manipulator Dynamics

We consider the well-known manipulator dynamics equation of motion

$$M(q)\ddot{q} + C(q, \dot{q})\dot{q} + G(q) = T + T_e, \quad (7)$$

where $M(q) \in \mathbb{R}^{n \times n}$ is the symmetric positive definite inertia matrix, $C(q, \dot{q}) \in \mathbb{R}^{n \times n}$ is a Coriolis matrix, $G(q) \in \mathbb{R}^n$ is a moment term due to gravity, $T \in \mathbb{R}^n$ is a control input given in torque, and $T_e \in \mathbb{R}^n$ is an external disturbance in torque. The (r, s) element of the matrix $C(q, \dot{q})$ is

$$C_{rs}(q, \dot{q}) = \frac{1}{2} \sum_{t=1}^n \left[\frac{\partial M_{rs}}{\partial q_t} \dot{q}_t + \frac{\partial M_{tr}}{\partial q_s} \dot{q}_t - \frac{\partial M_{ts}}{\partial q_r} \dot{q}_t \right], \quad (8)$$

see Li and Horowitz (1999). The Coriolis matrix calculated in this way satisfies the property that $\tilde{M} - 2C$ is skew-symmetric.

In the field of impedance control combined with operational space formulation, it is well known from Khatib (1987) that the robot dynamics (7) can be rewritten as

$$\begin{aligned} \tilde{M}(q)\dot{V}^b + \tilde{C}(q, \dot{q})V^b + \tilde{G}(q) &= \tilde{T} + \tilde{T}_e, \quad \text{where} \quad (9) \\ \tilde{M}(q) &= J_b(q)^{-T}M(q)J_b(q)^{-1}, \\ \tilde{C}(q, \dot{q}) &= J_b(q)^{-T}(C(q, \dot{q}) - M(q)J_b(q)^{-1}\dot{J})J_b(q)^{-1}, \\ \tilde{G}(q) &= J_b(q)^{-T}G(q), \quad \tilde{T} = J_b(q)^{-T}T, \quad \tilde{T}_e = J_b(q)^{-T}T_e. \end{aligned}$$

For compactness we use notation $(A^{-1})^T = A^{-T}$. Furthermore, we denote $\tilde{M}(q)$ as \tilde{M} , $\tilde{C}(q, \dot{q})$ as \tilde{C} and $\tilde{G}(q)$ as \tilde{G} . We also note that the manipulator dynamics of the workspace is based on the following assumption.

Assumption 1. The end-effector lies in a region $D \subset SE(3)$ such that J_b is full-rank, i.e., non-singular.

3. GEOMETRIC IMPEDANCE CONTROL ON $SE(3)$

3.1 Error Vector Derivation

In Lee et al. (2010), the authors suggest that an error function in $SO(3)$ can be chosen as

$$\psi_R(R, R_d) = \text{tr}(I - R_d^T R), \quad (10)$$

where $R \in SO(3)$ and $R_d \in SO(3)$ respectively represent the actual and desired rotation matrices. In $SO(3)$, the distance metric in (10) can also be defined using the Frobenius norm $\|\cdot\|_F$, as proposed in Huynh (2009),

$$\begin{aligned} \psi_R(R, R_d) &= \frac{1}{2}\|I - R_d^T R\|_F^2 \\ &= \frac{1}{2}\text{tr}((I - R_d^T R)^T(I - R_d^T R)). \end{aligned} \quad (11)$$

The formulation in (11) can be extended to general matrix groups. Therefore, we utilize the Frobenius norm to define an error function in $SE(3)$ as:

$$\Psi(g, g_d) = \frac{1}{2}\|I - g_d^{-1}g\|_F^2, \quad (12)$$

where $g \in SE(3)$ and $g_d \in SE(3)$ respectively represent the actual and desired configurations. Utilizing the homogeneous representation (1), it follows that

$$g = \begin{bmatrix} R & p \\ 0 & 1 \end{bmatrix}, \quad g_d = \begin{bmatrix} R_d & p_d \\ 0 & 1 \end{bmatrix}, \quad g^{-1} = \begin{bmatrix} R^T & -R^T p \\ 0 & 1 \end{bmatrix}. \quad (13)$$

This leads to the equivalent formulation for the error function $\Psi(g, g_d)$ in (12):

$$\Psi(g, g_d) = \text{tr}(I - R_d^T R) + \frac{1}{2}(p - p_d)^T(p - p_d). \quad (14)$$

This error function is related to the squared of the distance metric in $SE(3)$ proposed in Park (1995), in the sense that the error function in Park (1995) is also defined as a weighted summation of metrics in $SO(3)$ and the Euclidean space. However, in Park (1995) the bi-invariant metric $\|\log(R^T R_d)\|$ is utilized for $SO(3)$. In addition, the error function derived herein is the non-weighted version of one of the error functions proposed by Bullo and Murray (1999). We also emphasize that, by using the Frobenius norm-induced error function, we could justify the selection of the weighted error function in Bullo and Murray (1999). It is important to note that the $SE(3)$ error function (14) is left-invariant i.e.,

$$\Psi(g_l g, g_l g_d) = \frac{1}{2}\|I - g_d^{-1}g_l^{-1}g_l g\|_F^2 = \Psi(g, g_d), \quad (15)$$

where $g_l \in SE(3)$ is an arbitrary left translation. On the other hand, the right translation of the error function does not satisfy equation (14). Applying the right translations reads

$$\Psi(g g_r, g_d g_r) = \frac{1}{2}\|I - g_r^{-1}g_d^{-1}g g_r\|_F^2 \neq \Psi(g, g_d), \quad (16)$$

where $g_r \in SE(3)$ is an arbitrary right translation, which confirms that the error function is left-invariant. As suggested by Park (1995), it is natural to use body-frame coordinates for left-invariant error metrics in $SE(3)$.

To calculate the error vector in $SE(3)$, we perturb a configuration $g \in SE(3)$ with a right translation, as was done as in Lee et al. (2010) for $SO(3)$.

$$g_{\hat{\eta}} = g e^{\hat{\eta}\epsilon}, \quad \eta = \begin{bmatrix} \eta_1 \\ \eta_2 \end{bmatrix} \in \mathbb{R}^6 \implies \hat{\eta} \in \mathfrak{se}(3), \quad \epsilon \in \mathbb{R}, \quad (17)$$

where $\eta_1, \eta_2 \in \mathbb{R}^3$ refer to translational and rotational components, respectively. Therefore, the configuration variation can be represented by the homogeneous transformation matrix

$$\delta g_{\hat{\eta}} = g \hat{\eta} \implies \begin{bmatrix} \delta R & \delta p \\ 0 & 0 \end{bmatrix} = \begin{bmatrix} R \hat{\eta}_2 & R \eta_1 \\ 0 & 0 \end{bmatrix} \in T_g SE(3), \quad (18)$$

where $\hat{\eta}_2 \in \mathfrak{so}(3)$ and $T_g SE(3)$ represent tangent space of $SE(3)$ at configuration g . Expressing the error function (14) as

$$\Psi(g, g_d) = \frac{1}{2}\text{tr} \begin{bmatrix} 2I - R^T R_d - R_d^T R & * \\ * & (p - p_d)^T(p - p_d) \end{bmatrix},$$

where we utilize $*$ to denote the content of irrelevant matrix elements. Its perturbation can be obtained by

$$\begin{aligned} \delta \Psi(g, g_d) &= \frac{1}{2}\text{tr} \begin{bmatrix} -\delta R^T R_d - R_d^T \delta R & * \\ * & 2(p - p_d)^T \delta p \end{bmatrix} \\ &= \frac{1}{2}\text{tr} \begin{bmatrix} -\hat{\eta}_2^T R^T R_d - R_d^T R \hat{\eta}_2 & * \\ * & 2(p - p_d)^T R \eta_1 \end{bmatrix} \\ &= -\text{tr}(R_d^T R \hat{\eta}_2) + (p - p_d)^T R \eta_1 \\ &= (R_d^T R - R^T R_d)^\vee \cdot \eta_2 + (p - p_d)^T R \eta_1. \end{aligned} \quad (19)$$

We now define the *position* error vector e_g as

$$e_g = \begin{bmatrix} e_p \\ e_R \end{bmatrix} = \begin{bmatrix} R^T(p - p_d) \\ (R_d^T R - R^T R_d)^\vee \end{bmatrix} \in \mathbb{R}^6, \quad (20)$$

so that $\delta \Psi(g, g_d) = e_g^T \eta$ and

$$\hat{e}_g = \begin{bmatrix} R_d^T R - R^T R_d & R^T(p - p_d) \\ 0 & 0 \end{bmatrix} \in \mathfrak{se}(3). \quad (21)$$

As suggested in Lee et al. (2010), the tangent vectors $\dot{g} \in T_g SE(3)$ and $\dot{g}_d \in T_{g_d} SE(3)$ cannot be directly compared since they are not in the same tangent spaces. The desired velocity vector V_d^b defined in g_d can be translated into the vector V_d^* in g using the following formula (See Ch 2.4 of Murray et al. (1994) for the details of these steps):

$$\hat{V}_d^* = g_{ed} \hat{V}_d^b g_{ed}^{-1}, \quad \text{where } g_{ed} = g^{-1}g_d. \quad (22)$$

Additionally, it can be further represented as

$$V_d^* = \text{Ad}_{g_{ed}} V_d^b, \quad \text{with } \text{Ad}_{g_{ed}} = \begin{bmatrix} R_{ed} & \hat{p}_{ed} R_{ed} \\ 0 & R_{ed} \end{bmatrix}, \quad (23)$$

where $\text{Ad}_{g_{ed}} : \mathbb{R}^6 \rightarrow \mathbb{R}^6$ is an Adjoint map, $R_{ed} = R^T R_d$, and $p_{ed} = -R^T(p - p_d)$. Based on this, we define the *velocity* error vector e_V as

$$e_V = \underbrace{\begin{bmatrix} v^b \\ w^b \end{bmatrix}}_{V^b} - \underbrace{\begin{bmatrix} R^T R_d v_d + R^T R_d \hat{\omega}_d R_d^T (p - p_d) \\ R^T R_d \omega_d \end{bmatrix}}_{V_d^*} = \begin{bmatrix} e_v \\ e_\omega \end{bmatrix}. \quad (24)$$

It is also worth noting that

$$\begin{aligned} \dot{g} - \dot{g}_d(g_d^{-1}g) &= g\hat{V}^b - g_d\hat{V}_d g_d^{-1}g = g(\hat{V}^b - g^{-1}g_d\hat{V}_d g_d^{-1}g) \\ &= g\hat{e}_V \in T_g SE(3), \end{aligned} \quad (25)$$

which means that the velocity error vector e_V can be utilized to represent the error on the tangent space at g .

3.2 Impedance Control as a Dissipative Control

We consider the impedance control problem as a dissipative control design. Suppose that we have a Lyapunov function in a form that is similar to the total mechanical energy of the system

$$V(t, q, \dot{q}) = K(t, q, \dot{q}) + P(t, q), \quad (26)$$

where K and P are the kinetic and potential energy components of the Lyapunov function. Note that using total mechanical energy as a Lyapunov function is quite standard, as first proposed by Koditschek (1989). A desired property of the Lyapunov function is a dissipativity, i.e., $\dot{V}(t, q, \dot{q}) \leq 0$. The kinetic energy component of the Lyapunov function can be defined as follows

$$K(t, q, \dot{q}) = \frac{1}{2} e_V^T \tilde{M} e_V, \quad (27)$$

where $\tilde{M}(q)$ is defined in (9) and e_V is defined in (24).

One easy option for the potential component of the Lyapunov function is to the error function $\Psi(g, g_d)$ in (14) multiplied by a scalar. However, recent variable impedance control techniques require multiple and varying compliance gains along different coordinates Zhang et al. (2021); Martín-Martín et al. (2019). Therefore, we define a weighted version of the error function (14) as our potential function

$$\begin{aligned} P(t, q) &= \frac{1}{2} \text{tr}(\psi_k(g, g_d)^T \psi_k(g, g_d)), \text{ where} \\ \psi_k(g, g_d) &= \begin{bmatrix} \sqrt{K_R}(I - R_d^T R) & -\sqrt{K_p} R_d^T (p - p_d) \\ 0 & 0 \end{bmatrix}, \end{aligned} \quad (28)$$

$K_R \in \mathbb{R}^{3 \times 3}$, and $K_p \in \mathbb{R}^{3 \times 3}$ are symmetric positive definite stiffness matrices for orientation and translation, respectively. Then, using the fact that $\text{tr}(A) = \text{tr}(A^T)$, leads to

$$P(t, q) = \text{tr}(K_R(I - R_d^T R)) + \frac{1}{2}(p - p_d)^T R_d K_p R_d^T (p - p_d). \quad (29)$$

The potential function (29) is the second version of the multiple $SE(3)$ error function alternatives presented in Table. 1 of Bullo and Murray (1999), and it can be shown that it is left-invariant. Using the error vector e_g and e_V , an intuitive impedance control law that resembles conventional impedance controllers can be formulated as follows:

$$\tilde{T} = \tilde{M}\dot{V}_d^* + \tilde{C}V_d^* + \tilde{G} - K_g e_g - K_d e_V \quad (30)$$

where $K_g = \text{blkdiag}(K_p, K_R)$. Here, the $K_g e_g$ term can be interpreted as the spring force in $T_g^* SE(3)$, i.e., $f_g = K_g e_g$. However, the control action from (30) is not in the gradient direction of (26). Therefore, as shown in Bullo and Murray (1999), the elastic force f_g induced from the potential function (28), such that $f_g \in T_g^* SE(3)$, should be utilized and is given as follows:

$$f_g = \begin{bmatrix} f_p \\ f_R \end{bmatrix} = \begin{bmatrix} R^T R_d K_p R_d^T (p - p_d) \\ (K_R R_d^T R - R^T R_d K_R)^V \end{bmatrix} \quad (31)$$

The derivation of (31) is presented in the Appendix A. Using (31), a geometric impedance control law on $SE(3)$ is given by

$$\tilde{T} = \tilde{M}\dot{V}_d^* + \tilde{C}V_d^* + \tilde{G} - f_g - K_d e_V. \quad (32)$$

The proposed control design is based on the following assumption.

Assumption 2. The end-effector of the manipulator and the desired trajectory lies in the reachable set \mathcal{R} , i.e., $p(\theta) \in \mathcal{R} = \{p(\theta) \mid \forall \theta \in \mathbb{S}^n\} \subset \mathbb{R}^3$. The desired trajectory is also continuously differentiable.

The dissipative property of the impedance controller can be obtained by

$$\dot{V} = -e_V^T K_d e_V, \quad (33)$$

with the symmetric positive definite damping matrix $K_d \in \mathbb{R}^{6 \times 6}$. In order to obtain the control law, the time derivative of the Lyapunov function is considered as follows

$$\dot{V} = \dot{K} + \dot{P}. \quad (34)$$

The first term of the right hand side of (34) is calculated by using (23)-(24) as

$$\dot{K} = e_V^T \tilde{M}(q) \dot{e}_V + \frac{1}{2} e_V^T \dot{\tilde{M}}(q) e_V \quad (35)$$

with $\dot{e}_V = \dot{V}^b - \left(\frac{d}{dt} \text{Ad}_{g_{ed}}\right) V_d^b - \text{Ad}_{g_{ed}} \dot{V}_d^b = \dot{V}^b - \dot{V}_d^*$,

$$\frac{d}{dt} \text{Ad}_{g_{ed}} = \begin{bmatrix} \dot{R}_{ed} \hat{p}_{ed} R_{ed} + \hat{p}_{ed} \dot{R}_{ed} \\ 0 \end{bmatrix},$$

$$\dot{R}_{ed} = -\hat{\omega} R^T R_d + R^T R_d \hat{\omega}_d,$$

$$\dot{p}_{ed} = -\hat{\omega} R^T (p - p_d) + V^b - R^T R_d V_d^b.$$

We define the time derivative of the desired velocity $\dot{V}_d^* \triangleq \left(\frac{d}{dt} \text{Ad}_{g_{ed}}\right) V_d^b - \text{Ad}_{g_{ed}} \dot{V}_d^b$, so that $\dot{e}_V = \dot{V}^b - \dot{V}_d^*$. Then, by letting $\dot{T}_e = 0$ for control law derivation, equation (35) can be summarized as

$$\dot{K} = e_V^T \left(\tilde{T} - \tilde{C}V^b - \tilde{G} - \tilde{M}\dot{V}_d^* - \frac{1}{2} \dot{\tilde{M}} e_V \right). \quad (36)$$

For the potential energy counterpart, it can be shown that

$$\dot{P} = f_g^T e_V. \quad (37)$$

The derivation of (37) is shown in Appendix A.

The following Lemma turns out to be useful when deriving the control law.

Lemma 3. $\dot{\tilde{M}} - 2\tilde{C}$ is skew-symmetric.

Proof. See Chap. 3.5 of Lewis et al. (2003).

The following theorem shows that the proposed control law (32) satisfies the dissipative property of the impedance controller (33).

Theorem 4. Suppose assumptions 1 and 2 hold true. Consider a robotic manipulator with the dynamic equation of motions given by (7) and energy-based Lyapunov function candidate (26). Then, the Lyapunov function of the closed-loop system with the control law (32) satisfies dissipative property (33), when $T_e = 0$.

Proof. Plugging in the control law (32) into (36) and plugging in the resulting term into the Lyapunov (34), and using the velocity error (24) as well as *Lemma 3* leads to

$$\begin{aligned} \dot{V} &= e_V^T \left(\tilde{M}\dot{V}_d^* + \tilde{C}V_d^* - K_d e_V - \tilde{C}V^b - \tilde{M}\dot{V}_d^* - \frac{1}{2} \dot{\tilde{M}} e_V \right) \\ &= e_V^T \left(\frac{1}{2} \dot{\tilde{M}} - \tilde{C} - K_d \right) e_V = -e_V^T K_d e_V \leq 0, \end{aligned} \quad (38)$$

which shows that the closed-loop system is at least stable in the sense of Lyapunov (SISL), and shows proper

impedance behavior as proposed in Kronander and Billard (2016).

The asymptotic stability of closed loop system using a strict Lyapunov analysis as presented in the following Theorem 5.

Theorem 5. Suppose the assumptions 1 and 2 hold true. Consider a robotic manipulator with dynamic equations of motion given by (7), energy-based Lyapunov function (26), and the control law (32). Then, when $T_e = 0$, the equilibrium point $g(t) = g_d(t)$, such that $f_g = 0$, of the closed-loop system is asymptotically stable in the reachable set \mathcal{R} .

Proof. First, the time derivative of $f_g = [f_p^T, f_R^T]^T$ term is calculated as follows.

$$\begin{aligned} \dot{f}_g &= \begin{bmatrix} R^T R_d K_p R_d^T R & \hat{f}_p \\ 0 & \text{tr}(R^T R_d K_R) I - R^T R_d K_R \end{bmatrix} \begin{bmatrix} e_v \\ e_\Omega \end{bmatrix} \\ &\triangleq B_K(g, g_d) e_v. \end{aligned} \quad (39)$$

We denote $B_K(g, g_d) = B_K$ for the compactness of the notation. The derivation of (39) is presented in the Appendix A. By applying the control law (32) into (9) with $\tilde{T}_e = 0$, the error dynamics is

$$\begin{aligned} \dot{f}_g &= B_K e_v \\ \tilde{M} \dot{e}_V &= -\tilde{C} e_V - f_g - K_d e_V. \end{aligned} \quad (40)$$

Inspired by Bullo and Murray (1995) and as suggested in Lee et al. (2010), a Lyapunov function candidate V_1 for stability analysis can be defined as follows:

$$V_1 = V + \varepsilon f_g^T e_v, \quad \varepsilon > 0. \quad (41)$$

The time-derivative of V_1 using the Lyapunov function (38) the error dynamics (40) is

$$\begin{aligned} \dot{V}_1 &= -e_V^T K_d e_V + \varepsilon \dot{f}_g^T e_v + \varepsilon f_g^T \dot{e}_v \\ &= -e_V^T (K_d - \varepsilon B_K) e_V - \varepsilon f_g^T \tilde{M}^{-1} f_g \\ &\quad - \varepsilon f_g^T \tilde{M}^{-1} (\tilde{C} + K_d) e_V \end{aligned} \quad (42)$$

The matrix B_K is bounded by some constant a , i.e., $\|B_K\| \leq a$. This is because the reachable set is bounded, resulting in boundedness of f_p , and the term $(\text{tr}(R^T R_d K_R) I - R^T R_d K_R)$ is bounded as similarly as proposed in Lee et al. (2010). Therefore,

$$\begin{aligned} \dot{V}_1 &\leq -\|e_V\|_2^2 (\lambda_{\min}(K_d) - \varepsilon a) - \varepsilon \frac{1}{\lambda_{\max}(M)} \|f_g\|_2^2 \\ &\quad - \varepsilon \left(\frac{\|\tilde{C}\| + \lambda_{\min}(K_d)}{\lambda_{\max}(M)} \right) \|f_g\|_2 \|e_V\|_2 \\ &= -[\|f_g\|_2 \|e_V\|_2] \begin{bmatrix} \varepsilon c & \varepsilon b \\ \varepsilon b & k_d - \varepsilon a \end{bmatrix} \begin{bmatrix} \|f_g\|_2 \\ \|e_V\|_2 \end{bmatrix} \triangleq -z^T Q_\varepsilon z \end{aligned} \quad (43)$$

where $z = [\|f_g\|_2, \|e_V\|_2]^T \in \mathbb{R}^2$, $\lambda_{\min}(\cdot)$ and $\lambda_{\max}(\cdot)$ denotes the minimum and maximum eigenvalue of the matrix, respectively, $k_d = \lambda_{\min}(K_d)$, and

$$b = \frac{\|\tilde{C}\| + \lambda_{\min}(K_d)}{2\lambda_{\max}(M)}, \quad c = \frac{1}{\lambda_{\max}(M)}, \quad Q_\varepsilon = \begin{bmatrix} \varepsilon c & \varepsilon b \\ \varepsilon b & k_d - \varepsilon a \end{bmatrix} \in \mathbb{R}^{2 \times 2}.$$

With sufficiently large gains K_d, K_g and/or taking sufficiently small ε , one can make Q_ε positive definite. In particular, taking

$$\varepsilon < \min \left\{ \frac{k_d}{|a-c|}, \frac{k_d c}{b^2 + ac} \right\} \quad (44)$$

renders Q_ε positive definite, which completes the proof.

3.3 Impedance Control as an Exact Compensation Tracking Control Law

We now propose another geometric impedance control law utilizing the controller design techniques suggested by Sadegh and Horowitz (1990); Slotine and Li (1987) in order to attain a more robust stability result. First, a reference velocity \bar{V}_d and a reference acceleration $\dot{\bar{V}}_d$ is defined by

$$\begin{aligned} \bar{V}_d &= V_d^* - \lambda_g f_g \\ \dot{\bar{V}}_d &= \dot{V}_d^* - \lambda_g \dot{f}_g = \dot{V}_d - \lambda_g B_k e_V, \end{aligned} \quad (45)$$

where $\lambda_g \in \mathbb{R}_+$ is a positive scalar gain, but it is not restricted to the scalar. Then, a reference velocity error term \bar{e}_V can be defined accordingly as follows:

$$\bar{e}_V = V^b - \bar{V}_d = V^b - V_d^* + \lambda_g f_g = e_V + \lambda_g f_g \quad (46)$$

Using (46), we propose a second version of the geometric impedance control law in the following formulation:

$$\tilde{T} = \tilde{M} \dot{\bar{V}}_d + \tilde{C} \bar{V}_d - f_g - K_d \bar{e}_V + \tilde{G}. \quad (47)$$

The stability proof for the geometric impedance control law 2 is presented in the following theorem.

Theorem 6. Suppose the assumptions 1 and 2 hold true. Consider a robotic manipulator with dynamic equations of motion given by (7) and the control law (47). Then, when $T_e = 0$, the equilibrium point $g(t) = g_d(t)$, such that $f_g = 0$, of the closed-loop system is asymptotically stable in the reachable set \mathcal{R} .

Proof. We start the proof by defining the error dynamics under the control law (47).

$$\dot{f}_g = B_K (\bar{e}_V - \lambda_g f_g) \quad (48)$$

$$\tilde{M} \dot{\bar{e}}_V = -\tilde{C} \bar{e}_V - f_g - K_d \bar{e}_V$$

The energy-function-like Lyapunov function candidate $W(t, q, \dot{q})$ is defined by

$$\begin{aligned} W(t, q, \dot{q}) &= \bar{K}(t, q, \dot{q}) + P(t, q) \\ \bar{K}(t, q, \dot{q}) &= \frac{1}{2} \bar{e}_V^T \tilde{M} \bar{e}_V, \end{aligned} \quad (49)$$

The time-derivative of the Lyapunov function \dot{W} is evaluated based on (48) and Lemma 3 as follows:

$$\begin{aligned} \dot{W} &= \dot{\bar{K}} + \dot{P}, \quad \text{where} \\ \dot{\bar{K}} &= \bar{e}_V^T \left(\frac{1}{2} \tilde{M} \dot{\bar{e}}_V - \tilde{C} \bar{e}_V - f_g - K_d \bar{e}_V \right) \\ &= -\bar{e}_V^T f_g - \bar{e}_V^T K_d \bar{e}_V \\ \dot{P} &= f_g^T e_V = f_g^T (\bar{e}_V - \lambda_g f_g) = \bar{e}_V^T f_g - \lambda_g f_g^T f_g. \end{aligned} \quad (50)$$

Therefore, by using f_g and \bar{e}_V as the states of the Lyapunov function W ,

$$\dot{W} = -\bar{e}_V^T K_d \bar{e}_V - \lambda_g f_g^T f_g < 0 \quad (51)$$

which shows negative definiteness of \dot{W} , implying asymptotic stability.

We present some comments regarding the second version of the impedance control law in the following remark.

Remark 7. Comments on control law (47)

- (1) When control law (47) is utilized, the effective stiffness of the end-effector is changed. Therefore, one should choose the gains K_p and K_R carefully considering the effective stiffness.
- (2) When $\lambda_g \rightarrow 0$, the control law (47) becomes identical to (32).

- (3) The stability of the (32) is restricted by the selection of trajectories and gains because of its dependence on matrix norms such as $\|B_K\|$ and $\|\tilde{C}\|$, i.e., ε value sometimes needs to be small. On the other hand, for (47), λ_g is not dependent on these values, resulting in more generalized stability results.

4. SIMULATION RESULT

We utilize the UR5e robot model implemented in Matlab R2021a using Corke (2002). As a benchmark, we use a conventional impedance control from Zhu et al. (2020); Ochoa and Cortesão (2021); Shaw et al. (2022), which does not consider geometrical aspects, while allowing comparisons under similar initial conditions and gains to the controller presented in this paper. Specifically, the control law utilized for the benchmark is as follows:

$$\tilde{T}^s = \tilde{M}^s \dot{V}_d + \tilde{C}^s V + \tilde{G}^s - K_g e_g^s - K_d e_V^s \quad (52)$$

where \tilde{M}^s , \tilde{C}^s , and \tilde{G}^s can be obtained by replacing J_b by J_s , a spatial Jacobian matrix, from (9), and $\tilde{T}^s = J_s^{-T} T$. In addition, the spatial error vector e_g^s is defined as Zhu et al. (2020); Ochoa and Cortesão (2021); Shaw et al. (2022)

$$e_g^s = [(e_p^s)^T, (e_R^s)^T]^T, \quad \text{where} \quad (53)$$

$$e_p^s = x - x_d, \quad e_R^s = (r_{d1} \times r_1 + r_{d2} \times r_2 + r_{d3} \times r_3),$$

with $R = [r_1, r_2, r_3]$ and $R_d = [r_{d1}, r_{d2}, r_{d3}]$. Likewise, the spatial velocity error e_V^s is

$$e_V^s = \begin{bmatrix} v^s \\ \omega^s \end{bmatrix} - \begin{bmatrix} \dot{p}_d \\ \dot{\omega}_d^s \end{bmatrix} = V^s - V_d^s, \quad (54)$$

where the spatial velocity is obtained by $V^s = J_s \dot{q}$. Note that this controller is very similar to the one proposed in Caccavale et al. (1999), where the only difference is the representation of the rotational error e_R^s .

The simulations are conducted for a dynamic trajectory with a rapid motion tracking scenario. We present a simulation result with the first version of the geometric control law (32) since it enables a fair comparison with the benchmark controller. Additionally, we set the same desired impedance K_p , K_R , and K_d to both controllers and also let both controllers start at the same initial condition. The desired impedance gains are set as

$K_p = \text{diag}([200, 60, 80])$, $K_R = \text{diag}([10, 30, 100])$, $K_d = k_d I$ where $k_d = 50$. The initial point in the simulation is selected as

$$q(0) = [0.2, -0.5, 0.4, 0.6, -0.5, 0.2]^T,$$

$$\dot{q}(0) = [0, 0, 0, 0, 0, 0]^T.$$

The desired trajectories are

$$p_d(t) = \begin{bmatrix} -0.5 - 0.15 \cos 2t \\ 0.2 + 0.15 \sin 2t \\ 0.25 + 0.1 \sin t \end{bmatrix}, \quad R_d(t) = \begin{bmatrix} 1 & 0 & 0 \\ 0 & 0 & -1 \\ 0 & 1 & 0 \end{bmatrix} \quad (55)$$

The Cartesian trajectory tracking results are plotted in Fig. 1. The trajectory results in x - y plane are shown in Fig. 2. The RMS values for the performance metrics are shown in Tab. 1. Both the proposed control and benchmark control showed perfect trajectory tracking performance once after they were converged. However, the proposed control law improved performance in reducing the initial errors, especially in the translational part, as seen in

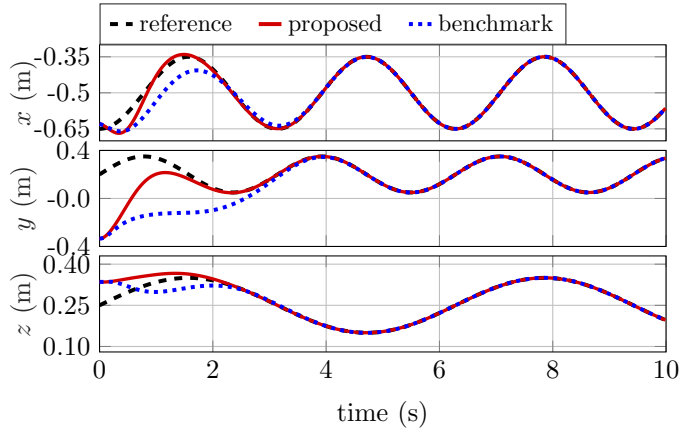


Fig. 1. The trajectory tracking results in x , y , and z coordinates for the proposed and benchmark approach are plotted.

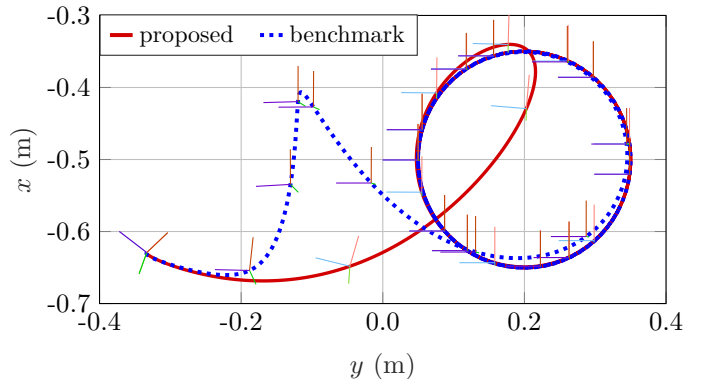


Fig. 2. Trajectory results in a bird-eye-view for $t = 0 \sim 10$ (s) with end-effector axes attached are plotted.

Table 1. Performance metrics in RMS values for the dynamic trajectory tracking scenario

Performance Metrics	Benchmark	Proposed
$\text{RMS}(x(t) - x_d(t))$	0.0317	0.0137
$\text{RMS}(y(t) - y_d(t))$	0.1992	0.1256
$\text{RMS}(z(t) - z_d(t))$	0.0183	0.0178
$\text{RMS}(P(t, q)), (28)$	6.5693	6.3624
$\text{RMS}(V(t, \dot{q})), (26)$	7.2622	6.6556

Tab. 1 and Fig. 2. This is mainly because the benchmark control tries to reduce the similar potential function separately in translational and orientational direction, while the proposed control approach reduces the translational and orientational error simultaneously.

The Matlab code for the implementation of the controller proposed in this paper is provided in <https://github.com/Joohwan-Seo/Geometric-Impedance-Control-Public>. Few remarks on the actual implementation are provided.

Remark 8. From the implementation perspective, the normal PD-like control with gravity compensation given by $\tilde{T} = -f_g(e_g) - K_d e_V + \tilde{G}$ can be utilized when the Jacobin matrix is numerically near singular. Similarly, $\tilde{T} = -K_g e_g - K_d e_V + \tilde{G}$ for the intuitive impedance control. This implies that even without dynamic parameters and solving inverse kinematics, we can solve the end-effector positioning problem, which has already been emphasized in an earlier work Hogan (1985).

5. CONCLUSION AND FUTURE WORKS

A novel impedance control law considering the geometric structure of the manipulator is proposed in this paper. The left-invariant error metric is first defined, and the geometrically consistent error vectors are derived. Based on the error vectors, the geometric impedance control rule is obtained from the dissipative property of the energy function. The stability analysis shows that the closed-loop system is asymptotically stable. In the simulation, we showed that the proposed control outperformed the conventional control in trajectory tracking.

In future work, we will combine the proposed geometric impedance control with reinforcement learning to solve robotic manipulation task problems. Since the controller is now defined appropriately, we expect an improvement in performance compared to state-of-the-art methods. We will also show that task encoding based on a geometrically consistent error vector is useful. Above that, we will also research the solution of robotic tasks where the tasks can be better encoded as velocity fields instead of desired trajectories, i.e., a closed-loop system lying on the desired manifold.

REFERENCES

- Abu-Dakka, F.J. and Saveriano, M. (2020). Variable impedance control and learning—a review. *Frontiers in Robotics and AI*, 7, 590681.
- Abu-Dakka, F.J. et al. (2018). Force-based variable impedance learning for robotic manipulation. *Robotics and Autonomous Systems*, 109, 156–167.
- Bullo, F. and Murray, R.M. (1995). Proportional derivative (pd) control on the euclidean group.
- Bullo, F. and Murray, R.M. (1999). Tracking for fully actuated mechanical systems: a geometric framework. *Automatica*, 35(1), 17–34.
- Caccavale, F. et al. (1999). Six-dof impedance control based on angle/axis representations. *IEEE Transactions on Robotics and Automation*, 15(2), 289–300.
- Chen, H. and Liu, Y. (2013). Robotic assembly automation using robust compliant control. *Robotics and Computer-Integrated Manufacturing*, 29(2), 293–300.
- Corke, P. (2002). Robotics toolbox. *Obtained from Peter O. Corke site: <http://www.petercorke.com/Robotics%20Toolbox.html>*.
- Duan, J. et al. (2018). Adaptive variable impedance control for dynamic contact force tracking in uncertain environment. *Robotics and Autonomous Systems*, 102, 54–65.
- Fasse, E.D. and Broenink, J.F. (1997). A spatial impedance controller for robotic manipulation. *IEEE Transactions on Robotics and Automation*, 13(4), 546–556.
- Hogan, N. (1985). Impedance control: An approach to manipulation: Part ii—implementation.
- Huynh, D.Q. (2009). Metrics for 3d rotations: Comparison and analysis. *Journal of Mathematical Imaging and Vision*, 35(2), 155–164.
- Khan, S.G. et al. (2010). Safe adaptive compliance control of a humanoid robotic arm with anti-windup compensation and posture control. *International Journal of Social Robotics*, 2(3), 305–319.
- Khatib, O. (1987). A unified approach for motion and force control of robot manipulators: The operational space formulation. *IEEE Journal on Robotics and Automation*, 3(1), 43–53.
- Koditschek, D.E. (1989). The application of total energy as a lyapunov function for mechanical control systems. *Contemporary mathematics*, 97, 131.
- Kronander, K. and Billard, A. (2016). Stability considerations for variable impedance control. *IEEE Transactions on Robotics*, 32(5), 1298–1305.
- Lee, T. et al. (2010). Geometric tracking control of a quadrotor uav on se (3). In *49th IEEE conference on decision and control (CDC)*, 5420–5425. IEEE.
- Lewis, F.L. et al. (2003). *Robot manipulator control: theory and practice*. CRC Press.
- Li, P.Y. and Horowitz, R. (1999). Passive velocity field control of mechanical manipulators. *IEEE Transactions on robotics and automation*, 15(4), 751–763.
- Li, Y. et al. (2010). Learning compliance control of robot manipulators in contact with the unknown environment. In *2010 IEEE International Conference on Automation Science and Engineering*, 644–649. IEEE.
- Luo, J. et al. (2019). Reinforcement learning on variable impedance controller for high-precision robotic assembly. In *2019 International Conference on Robotics and Automation (ICRA)*, 3080–3087. IEEE.
- Lynch, K.M. and Park, F.C. (2017). *Modern robotics*. Cambridge University Press.
- Martín-Martín, R. et al. (2019). Variable impedance control in end-effector space: An action space for reinforcement learning in contact-rich tasks. In *2019 IEEE/RSJ International Conference on Intelligent Robots and Systems (IROS)*, 1010–1017. IEEE.
- Murray, R.M., Li, Z., Sastry, S.S., and Sastry, S.S. (1994). *A mathematical introduction to robotic manipulation*. CRC press.
- Ochoa, H. and Cortesão, R. (2021). Impedance control architecture for robotic-assisted mold polishing based on human demonstration. *IEEE Transactions on Industrial Electronics*, 69(4), 3822–3830.
- Ott, C. et al. (2008). On the passivity-based impedance control of flexible joint robots. *IEEE Transactions on Robotics*, 24(2), 416–429.
- Park, F.C. (1995). Distance metrics on the rigid-body motions with applications to mechanism design.
- Rashad, R. et al. (2019). Energy tank-based wrench/impedance control of a fully-actuated hexarotor: A geometric port-hamiltonian approach. In *2019 International Conference on Robotics and Automation (ICRA)*, 6418–6424. IEEE.
- Rozo, L. et al. (2016). Learning physical collaborative robot behaviors from human demonstrations. *IEEE Transactions on Robotics*, 32(3), 513–527.
- Sadegh, N. and Horowitz, R. (1990). Stability and robustness analysis of a class of adaptive controllers for robotic manipulators. *The International Journal of Robotics Research*, 9(3), 74–92.
- Shaw, S., Abbatematteo, B., and Konidakis, G. (2022). Rmps for safe impedance control in contact-rich manipulation. In *2022 International Conference on Robotics and Automation (ICRA)*, 2707–2713. IEEE.
- Slotine, J.J.E. and Li, W. (1987). On the adaptive control of robot manipulators. *The international journal of*

robotics research, 6(3), 49–59.

Stramigioli, S. and Duindam, V. (2001). Variable spatial springs for robot control applications. In *IROS*, 1906–1911.

Zhang, X. et al. (2021). Learning variable impedance control via inverse reinforcement learning for force-related tasks. *IEEE Robotics and Automation Letters*, 6(2), 2225–2232.

Zhu, Y. et al. (2020). robosuite: A modular simulation framework and benchmark for robot learning. In *arXiv preprint arXiv:2009.12293*.

Appendix A

A.1 A derivation of geometric elastic force f_g (31)

Similar to (19), the potential function (28) is perturbed as follows:

$$\delta P = -\text{tr}(K_R R_d^T R \hat{\eta}_2) + (p - p_d)^T R_d K_p R_d^T R \eta_1$$

The first term in the equation above is further evaluated as

$$\begin{aligned} -\text{tr}(K_R R_d^T R \hat{\eta}_2) &= -\frac{1}{2} \text{tr}((K_R R_d^T R - R^T R_d K_R) \hat{\eta}_2) \\ &= (K_R R_d^T R - R^T R_d K_R)^\vee \cdot \eta_2 = f_R^T \eta_2, \end{aligned}$$

where $-\frac{1}{2} \text{tr}(\hat{x} \hat{y}) = x^T y$ is utilized. The second term can be similarly represented using $f_p = R^T R_d K_p R_d^T (p - p_d)$. The perturbed potential function can be notated as follows:

$$\delta P = f_p^T \eta_1 + f_R^T \eta_2 = \begin{bmatrix} f_p^T & f_R^T \end{bmatrix} \begin{bmatrix} \eta_1 \\ \eta_2 \end{bmatrix} = f_g^T \eta.$$

Since η is arbitrary, we can represent an elastic force in $SE(3)$ with respect to the potential function (28) as f_g .

A.2 A derivation of the time-derivative of the potential energy part (37)

The time-derivative of the potential function is

$$\frac{dP}{dt} = \frac{1}{2} \text{tr}(\dot{\psi}_k^T \psi_k) + \frac{1}{2} \text{tr}(\psi_k^T \dot{\psi}_k) = \text{tr}(\psi_k^T \dot{\psi}_k)$$

Where,

$$\begin{aligned} \dot{\psi}_k &= \frac{d\psi_k}{dt} = \begin{bmatrix} -\sqrt{K_R} R_d^T R \hat{e}_\Omega & m_{12} \\ 0 & 0 \end{bmatrix}, \text{ with} \\ m_{12} &= \sqrt{K_p} \hat{\omega}_d R_d^T (p - p_d) - \sqrt{K_p} R_d^T R v + \sqrt{K_p} v_d. \end{aligned}$$

Which leads to the form of

$$\frac{dP}{dt} = \text{tr} \left(\begin{bmatrix} a_{11} & * \\ * & a_{22} \end{bmatrix} \right)$$

where $*$ terms are not of interest because of the trace operator.

$$\begin{aligned} a_{11} &= (I - R^T R_d) \sqrt{K_R}^T (-\sqrt{K_R}) R_d^T R \hat{e}_\Omega \\ a_{22} &= -(p - p_d)^T R_d \sqrt{K_p}^T m_{12} \end{aligned}$$

Using the assumption that K_R is a symmetric positive definite matrix, and matrices are commutable in the trace, i.e., $\text{tr}(AB) = \text{tr}(BA)$,

$$\begin{aligned} \text{tr}(a_{11}) &= -\text{tr}((I - R^T R_d) K_R R_d^T R \hat{e}_\Omega) \\ &= -\text{tr}(K_R R_d^T R \hat{e}_\Omega) + \text{tr}(R^T R_d K_R R_d^T R \hat{e}_\Omega), \end{aligned}$$

where the second term is evaluated as

$$\text{tr}(R^T R_d K_R R_d^T R \hat{e}_\Omega) = 0$$

from the fact that $\text{tr}(AB) = \text{tr}(B^T A^T) = \text{tr}(A^T B^T) = -\text{tr}(AB)$ with $A^T = A$ and $B^T = -B$. Then, the remaining term is

$$\begin{aligned} \text{tr}(a_{11}) &= -\frac{1}{2} \text{tr}(K_R R_d^T R \hat{e}_\Omega) + \frac{1}{2} \text{tr}(R^T R_d K_R \hat{e}_\Omega) \\ &= -\frac{1}{2} \text{tr}((K_R R_d^T R - R^T R_d K_R) \hat{e}_\Omega) = f_R^T \hat{e}_\Omega \end{aligned}$$

On the other hand, $\text{tr}(a_{22}) = a_{22}$ can be unraveled as

$$\begin{aligned} a_{22} &= -(p - p_d)^T R_d K_p \hat{\omega}_d R_d^T (p - p_d) \\ &+ (p - p_d)^T R_d K_p R_d^T R v - (p - p_d)^T R_d K_p v_d \\ &= -(p - p_d) R_d K_p R_d^T R R^T R_d \hat{\omega}_d R_d^T (p - p_d) \\ &+ (p - p_d)^T R_d K_p R_d^T R (v - R^T R_d v_d) \\ &= (p - p_d)^T R_d K_p R_d^T R (v - R^T R_d v_d - R^T R_d \hat{\omega}_d R_d^T (p - p_d)) \\ &= f_p e_v. \end{aligned}$$

Putting all things together,

$$\frac{dP}{dt} = \begin{bmatrix} f_p^T & f_R^T \end{bmatrix} \begin{bmatrix} e_v \\ e_\Omega \end{bmatrix} = f_g^T e_v,$$

which is (37), where f_g is defined in (31).

A.3 Derivation of \dot{f}_g (39)

The time derivative of f_R is

$$\dot{f}_R = \frac{d}{dt} (K_R R_d^T R - R^T R_d K_R)^\vee, \text{ where}$$

$$\begin{aligned} &\frac{d}{dt} (K_R R_d^T R - R^T R_d K_R) \\ &= K_R (\hat{\omega}_d^T R_d R + R_d R \hat{\omega}) - (\hat{\omega}^T R^T R_d + R^T R_d \hat{\omega}_d) K_R \\ &= K_R (-\hat{\omega}_d R_d R + R_d R \hat{\omega}) + (\hat{\omega} R^T R_d - R^T R_d \hat{\omega}_d) K_R \\ &= K_R R_d^T R \hat{e}_\Omega + \hat{e}_\Omega R^T R_d K_R. \end{aligned}$$

Therefore,

$$\begin{aligned} \dot{f}_R &= (K_R R_d^T R \hat{e}_\Omega + \hat{e}_\Omega R^T R_d K_R)^\vee \\ &= (\text{tr}(R^T R_d K_R) I - R^T R_d K_R) \hat{e}_\Omega, \end{aligned}$$

where the following useful lemma is utilized.

Lemma 9. For $A \in \mathbb{R}^{3 \times 3}$, $b \in \mathbb{R}^3$,

$$(A \hat{b} + \hat{b} A^T)^\vee = (\text{tr}(A^T) I - A^T) b.$$

The time derivative of f_p is

$$\begin{aligned} \dot{f}_p &= \frac{d}{dt} (R^T R_d K_p R_d^T (p - p_d)) \\ &= -\hat{\omega} R^T R_d K_p R_d^T (p - p_d) + R^T R_d \hat{\omega}_d K_p R_d^T (p - p_d) \\ &\quad - R^T R_d K_p \hat{\omega}_d R_d (p - p_d) + R^T R_d K_p R_d^T (R v - R_d v_d) \\ &= -\underbrace{(\hat{\omega} - R^T R_d \hat{\omega}_d R_d^T R)}_{\hat{e}_\Omega} \underbrace{R^T R_d K_p R_d^T (p - p_d)}_{f_p} \\ &\quad + R^T R_d K_p R_d^T R \underbrace{(v - R^T R_d v_d - R^T R_d \hat{\omega}_d R_d^T (p - p_d))}_{e_v} \\ &= -\hat{e}_\Omega f_p + R^T R_d K_p R_d^T R e_v = \hat{f}_p e_\Omega + R^T R_d K_p R_d^T R e_v. \end{aligned}$$

Combining with the previous result, it is shown that

$$\begin{aligned} \dot{f}_g &= \begin{bmatrix} R^T R_d K_p R_d^T R & \hat{f}_p \\ 0 & \text{tr}(R^T R_d K_R) I - R^T R_d K_R \end{bmatrix} \begin{bmatrix} e_v \\ e_\Omega \end{bmatrix} \\ &= B_K(g, g_d) e_v. \end{aligned}$$